Paper No.
11027

NACE INTERNATIONAL CORROSION 2018 Conference & Expo

Formation Mechanisms of Iron Oxide and Iron Sulfide at High Temperature in H_2S Corrosion Environment

Shujun Gao, Bruce Brown, David Young, Srdjan Nesic, Marc Singer
Institute for Corrosion and Multiphase Technology
Department of Chemical & Biomolecular Engineering, Ohio University
342 West State Street
Athens, OH, 45701
USA

ABSTRACT

The mechanisms of corrosion of mild steel, and associated corrosion product formation, in high temperature sour environments are still largely unknown although they directly relate to pressing operating issues in the oil and gas industry. Previous studies have shown that, from 80°C to 200°C in an H_2S only environment, magnetite forms as an inner layer while iron sulfides are found in the outer layer. Although magnetite is thermodynamically less stable than iron sulfide, it was always observed as a defined inner layer. In this work, experiments were conducted to investigate the formation mechanisms of magnetite and iron sulfide in a H_2S environment at high temperature. The corrosion behavior of mild steel was first investigated in environments with and without H_2S at 120°C, showing that magnetite is the dominant corrosion product layer in the initial stages of corrosion, due to a much faster kinetics of formation than iron sulfide (mackinawite). Magnetite is assumed to be responsible for the initial rapid decrease of the corrosion rate in this environment. In another experiment, the conversion of magnetite into mackinawite was investigated by exposing a preformed magnetite layer on an inert steel substrate (nickel) to an H_2S environment. Consequently, it is postulated that Fe_3O_4 experiences a simultaneous and continuous process of formation at the steel/magnetite interface and conversion to mackinawite at the magnetite/mackinawite interface. A descriptive model for the formation mechanisms of magnetite and iron sulfide at high temperature is presented.

Key words*: hydrogen sulfide, high temperature corrosion, iron sulfide, magnetite*

INTRODUCTION

Persistent energy demand moves the exploration and production of hydrocarbons towards ever deeper and harsher reservoirs, both onshore and offshore. These wells are frequently operated under high temperature and high pressure conditions in the presence of H_2S.[1-4] As a result, these operating environments present a constant challenge for new developments in materials selection, design technology, corrosion management, and corrosion modeling in the oil and gas industry.[5-8]

H_2S corrosion at low temperature (< 80°C) has been extensively investigated in the past decades; some of the key issues have been well understood.[9-13] However, at elevated temperatures (> 80°C), the

mechanisms of H_2S corrosion have not been sufficiently studied and many aspects of corrosion kinetics and layer formation processes remain unclear.

The author's previous research conducted at four elevated temperatures levels, 80°C, 120°C, 160°C, and 200°C, has shown that the initial corrosion rate increases with increasing temperature while the final stable corrosion rate decreased with temperature.[14,15] Mackinawite, troilite, pyrrhotite, and pyrite were identified as the main iron sulfide phases in the outer layer at 80°C, 120°C, 160°C and 200°C, respectively. Iron oxide was detected as an inner layer at every studied temperature and was later identified as magnetite (Fe_3O_4) by electron diffraction performed in a transmission electron microscope (TEM).[16] Thermodynamically, Fe_3O_4 is less stable than any iron sulfide and should not be present in an H_2S dominated environment.[13] Indeed, it was never reported in similar environments at low temperature.[17] However, further experiments with different test durations, ranging from 1 to 21 days, showed that Fe_3O_4 does not disappear as expected based on thermodynamic arguments, and was persistently found as an inner layer with a relatively constant thickness of 25 µm,[17] as shown in Figure 1.

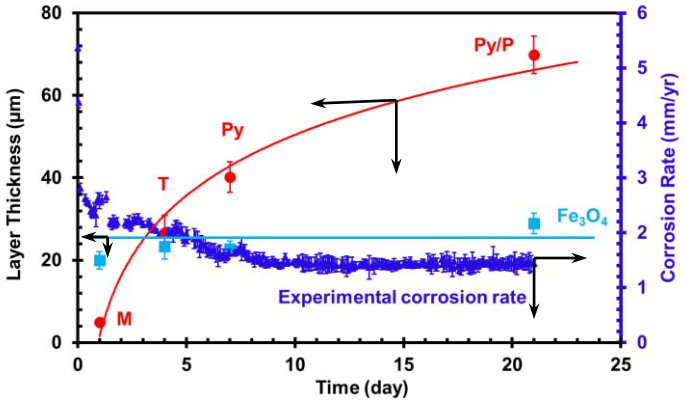

Figure 1. Corrosion rate and layer thickness of Fe_3O_4 and iron sulfide change with time, T=120°C, pH_2S=0.1 bar, pH=4.0 (initial) ~ 5.5 (final), M: mackinawite, T: troilite, Py: pyrrhotite, P: pyrite.[17]

Reviewing these results, two interesting gaps in understanding can be identified:

1. The corrosion rate quickly decreased in the first day from 5.5 to 2 mm/yr (see dark blue data points in Figure 1). Yet, it is not entirely clear which layer, Fe_3O_4 or mackinawite, was responsible for the decrease of the corrosion rate. Was there a sequence in the layer formation? How fast are these layers forming?

2. The thickness of inner Fe_3O_4 layer did not change significantly with time (20 to 30 µm from day 1 to day 21), while the outer iron sulfide layer kept growing with time from 5 µm to reach 90 µm after 21 days (see light blue and red data points in Figure 1). So what was the layer growth mechanism of iron sulfide in the presence of a Fe_3O_4 layer?

HYPOTHESES

The following hypotheses were proposed to address the above two questions:

1st Hypothesis: At high temperature, Fe_3O_4 forms very quickly during the initial stages of corrosion. It is a protective layer that slows down the corrosion rate. Therefore, the growth of the Fe_3O_4 layer gradually slows down as the lower corrosion rates slow down the formation rate Fe_3O_4. At the same time the

conversion of Fe_3O_4 to FeS proceeds at a steady state until a balance is established and the thickness of the Fe_3O_4 becomes constant.

2nd Hypothesis: Iron sulfide growth mechanism is mainly through a conversion from Fe_3O_4. The Fe_3O_4 simultaneously forms at the steel/Fe_3O_4 interface and converts to FeS at the Fe_3O_4/FeS interface.

METHODOLOGY

To test the 1st hypothesis, Experimental Set #1 was conducted, as shown in Figure 2:

- Step 1: A X65 carbon steel specimen was immersed into 1 wt.% NaCl solution (purged by N_2) without H_2S. The experimental condition was 120°C at an initial pH 4.0. After 1 day, the specimen with preformed Fe_3O_4 layer were retrieved, dried and stored in a nitrogen atmosphere.

- Step 2: The preformed Fe_3O_4 carbon steel specimen were exposed under the same condition (1 wt.% NaCl solution, 120°C, initial pH 4.0) containing 0.1 bar H_2S, for 1 day.

According to the 1st hypothesis, the iron sulfide layer growth should be dominant in Step 2, since the initial Fe_3O_4 layer formation step would have already been completed. Therefore, a much thicker iron sulfide (mackinawite) layer would form compared with the same experiment conducted with no preformed Fe_3O_4 layer (see Figure 2 and the first point in Figure 1).

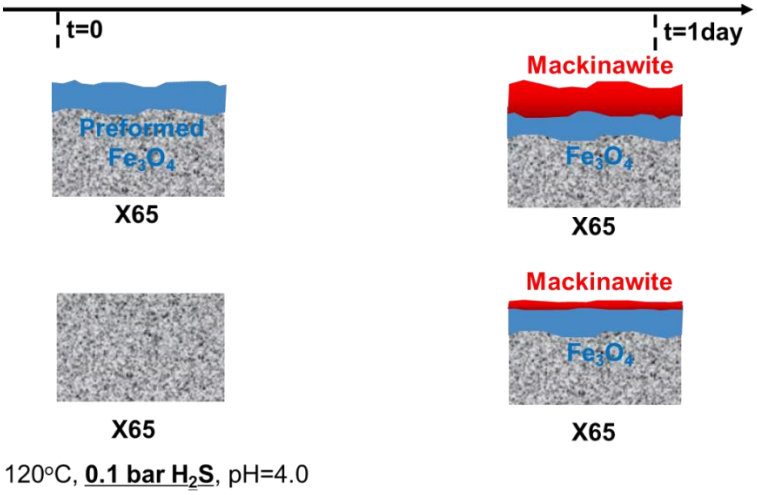

Figure 2. Experiment design to test hypothesis #1.

To verify the 2nd hypothesis, the Experimental Set #2 was performed, as shown in Figure 3:

- Step 1: Nickel (Ni) specimens, which should not corrode in the current experimental conditions with or without H_2S, were immersed into a 1 wt.% NaCl solution (purged by N_2) without H_2S. Some X65 steel specimens were also immersed in the cell at the same time solely to act as a source of Fe^{2+}. The test condition was still 120°C at an initial pH 4.0. This was done in order to precipitate Fe_3O_4 on the Ni surface via Reaction (1):

$$3Fe^{2+} + 4H_2O \rightarrow Fe_3O_4 + 8H^+ + 2e^- \quad (1)$$

The cathodic reaction(s) associated with Reaction (1) is not identified with certainty as of yet but it is postulated that H^+ reduction and H_2S reduction could be involved.

- Step 2: The Ni specimens with preformed Fe_3O_4 were exposed to a 0.1 bar H_2S environment under the same conditions (120°C, initial pH 4.0) for 1 day.

Based on the 2nd hypothesis, the preformed Fe_3O_4 layer should convert to iron sulfide in Step 2, via Reaction (2). Since there was no replenishment for Fe from the steel substrate to form new Fe_3O_4 (Reaction (1)), the Fe_3O_4 found at the end of Step 2 should be either very thin or even non-existent if it completely converted to iron sulfide.

$$Fe_3O_4 + 3H_2S + 2H^+ + 2e^- \rightarrow 3FeS + 4H_2O \quad (2)$$

The anodic reaction(s) associated with Reaction (2) is also not clearly identified but Fe oxidation and/or reaction (1) are likely.

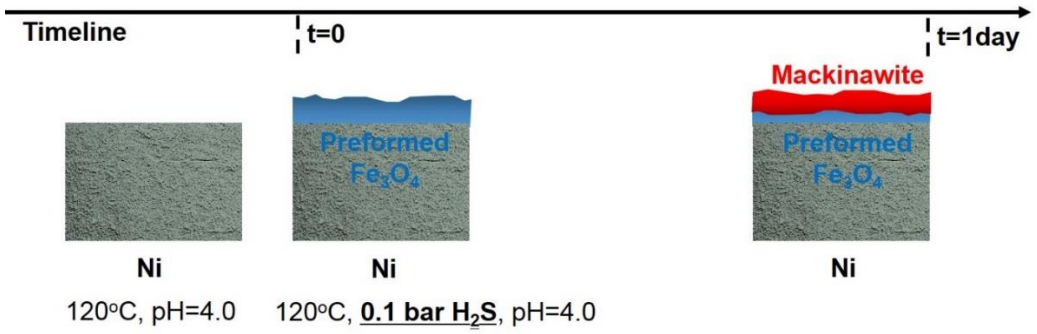

Figure 3. Experiment design to test hypothesis #2.

H_2S corrosion experiments were conducted in a 7 L Hastelloy autoclave, shown in Figure 4. Linear polarization resistance (LPR) measurements were carried out in a conventional three-electrode electrochemical setup using a potentiostat. The working electrode was a cylindrical UNS K03014 (API 5L X65) carbon steel, its chemical composition is shown in Table 1. A Pt-coated Nb cylinder served as the counter electrode. Due to the lack of a reliable reference electrode in the high temperature H_2S environment, a commercial Zr/ZrO_2 high-temperature, high-pressure electrode within the pH probe was used as a pseudo-reference electrode. This is doable as long as its potential is stable under the experimental conditions, while the exact potential with respect to a SHE is unknown).[18] Some flat specimens were fastened to a fixed shaft using a PTFE-coated 304SS wire. A centrally positioned impeller with 1000 rpm rotation speed was used to keep the solution well mixed during each experiment.

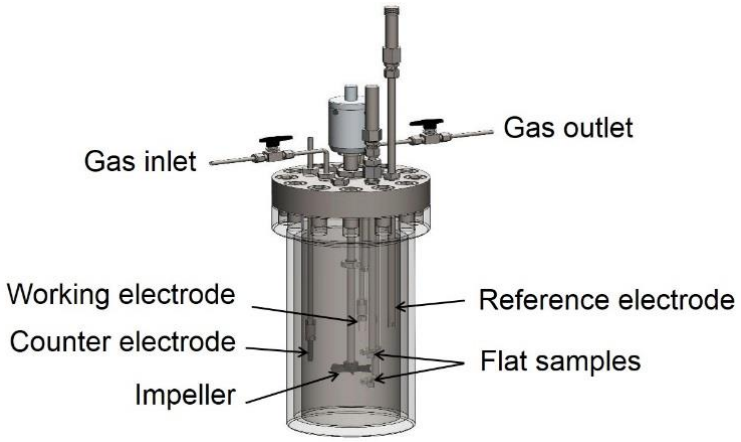

Figure 4. Experimental autoclave setup.

Table 1. Chemical composition of API 5L X65 carbon steel (wt. %).

Cr	Mo	S	V	Si	C	P	Ni	Mn	Fe
0.14	0.16	0.009	0.047	0.26	0.13	0.009	0.36	1.16	Balance

The experimental conditions such as pH and pH_2S, summarized in Table 2, were calculated based on an in-house water chemistry model (reviewed in previous publications)[14]. Before each experiment, the carbon steel specimens were polished with 400# and 600# grit abrasive paper, then thoroughly rinsed with deionized water and isopropanol. The 1 wt.% NaCl solution was purged with N_2 overnight at room temperature. Then the pH was adjusted according to the water chemistry calculation and H_2S added to the autoclave at room temperature to achieve a solution pH of 4.0 and desired 0.1 bar pH_2S when the temperature reached 120°C. After each experiment, the corroded specimens were retrieved and examined by X-ray diffraction (XRD), scanning electron microscopy/energy dispersive X-ray spectroscopy (SEM/EDS). Other experimental details can be found elsewhere.[14] For the tests without H_2S, the same procedure was followed except that no H_2S was involved.

Table 2. Test matrix for the effect of temperature

Parameter	Value
Temperature	120 °C
pH_2S	0.1 bar
Initial pH	4.0
Rotation speed	1000 rpm

RESULTS

Sequence of Fe_3O_4/FeS Formation

The corrosion rates obtained in Experimental Set #1 with H_2S (0.1 bar), and without H_2S, are shown in Figure 5. For clarity, these two are respectively labeled as experiment "with H_2S", "without H_2S" and "with preformed Fe_3O_4".

Looking first at the results from experiment "with H_2S" and experiment "without H_2S", the LPR corrosion rates are both shown to decrease relatively quickly at high temperature. The LPR corrosion rate from experiment "without H_2S" gradually decreased during the first 50 hours of exposure and reached a stable corrosion rate of 0.5 mm/yr. The LPR corrosion rate from experiment "with H_2S" reduced dramatically in the first 2 hours from over 5 mm/yr to about 2.8 mm/yr. Then it kept decreasing in a slower manner and eventually stabilized around 1 mm/yr.

The results from experiment "with preformed Fe_3O_4" are plotted in red in Figure 5, including the 1 day, representing the time needed to preform the Fe_3O_4 layer. The corrosion rates experienced by the specimen during the Fe_3O_4 layer formation (red dots in Figure 5) are the same to the corrosion rates during the first day of the experiment "without H_2S" (green dots in Figure 5) as would be expected. After the specimen with the preformed Fe_3O_4 was transferred to the H_2S environment at the 1-day mark, the LPR corrosion rate in the experiment "with preformed Fe_3O_4" started at 3.5 mm/yr, which is lower than the initial LPR rate obtained the experiment "with H_2S" (5.5 mm/yr). This result demonstrates that the Fe_3O_4 layer alone offers additional protection in an H_2S environment. The relatively high initial corrosion rate (3.5 mm/yr) value could be due to some cracking and/or spalling, created when the specimen was transferred, as the Fe_3O_4 layer was expected to provide higher initial corrosion protection in the H_2S

environment. The corrosion rate did decrease sharply in the next few hours of exposure but stabilized at 1.8 mm/yr, similarly to the final rate in the experiment "with H_2S". In comparison, a higher protectiveness by the Fe_3O_4 layer was clearly demonstrated in an environment without H_2S at the same high temperature.[19]

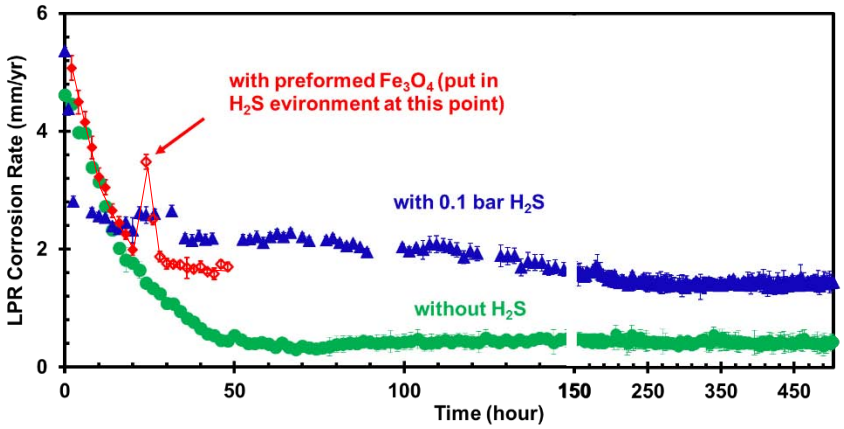

Figure 5. LPR corrosion rate in experiments without H_2S (green), with 0.1 bar H_2S (blue), and with preformed Fe_3O_4 layer for one-day, T=120°C, initial pH=4.0, B=23 mV/decade.

The corrosion products from the experiment "without H_2S" at high temperature were characterized by X-ray diffraction (XRD) after different test durations, as shown in Figure 6. All the corrosion products were identified as pure magnetite (Fe_3O_4) regardless of the exposure time. The EDS mapping scan, Figure 7, also confirms that the layer was comprised of iron (Fe) and oxygen (O). The intensity of the peaks also did not increase with time and the α-Fe matrix was already undetectable after the 1 day experiment. This means that the Fe_3O_4 became very thick and compact rapidly, implying good corrosion protection properties. The thickness after 1 day of exposure was approximately 25 µm, which is appropriately the same value as the thickness of the oxide layer obtained from experiment "with H_2S" for 1 day, as shown in Figure 1 and Figure 7. The fact that the two Fe_3O_4 layer thicknesses are the same seems to indicate that the Fe_3O_4 growth during the first day of testing occurs with little interference from H_2S. Consequently, it is proposed that the Fe_3O_4 formation dominated the first few hours of testing at high temperature and that the Fe_3O_4 layer rapidly reached its steady state thickness, even with H_2S. This is discussed in more details below.

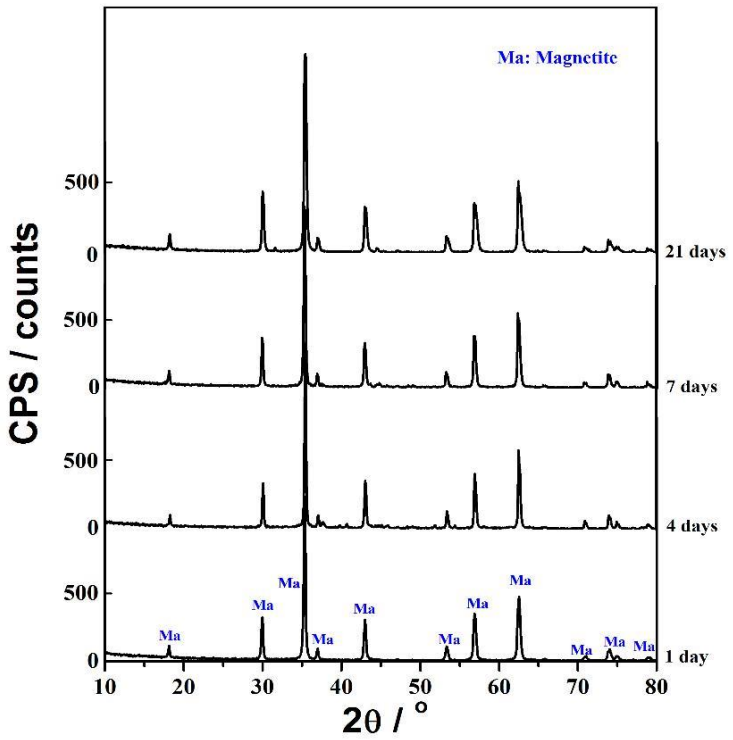

Figure 6. XRD patterns of X65 specimen in experiment without H_2S after different test durations, T=120°C, initial pH=4.0.

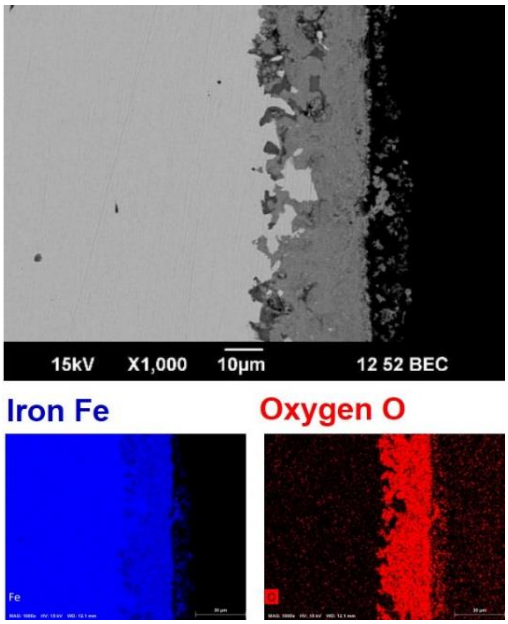

Figure 7. Cross-section and EDS mapping results for X65 specimen in experiment without H_2S after 1 day, T=120°C, initial pH=4.0.

The cross-sections of specimens from the experiment "without H_2S" are shown in Figure 8. It can be seen that the overall layer thickness increased from 25 μm after 1 day to 80 μm after 21 days. Figure 9 shows that, the Fe_3O_4 layer growth in experiment "without H_2S" follows almost the same trend as the mixed FeS/Fe_3O_4 corrosion product layer growth in the experiment "with H_2S" displayed in Figure 1. This could be a coincidence, especially since the thickness of the Fe_3O_4 layer alone stayed at ~25 μm in the experiment "with H_2S" and did not increase further with exposure time. However, this could also

indicate that the FeS and the Fe_3O_4 formation rates are inherently linked. This, again, highlights the complexity of the growth mechanism of iron sulfide in the presence of a Fe_3O_4 layer, which will be discussed later.

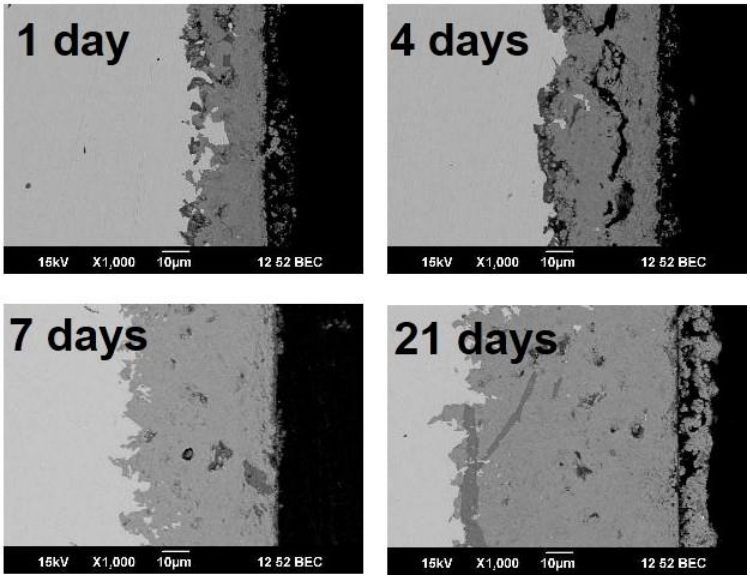

Figure 8. The growth of Fe_3O_4 layer with time, shown by cross-sections of X65 specimen in the experiment without H_2S after different test durations (obtained in separate experiments), T=120°C, initial pH=4.0.

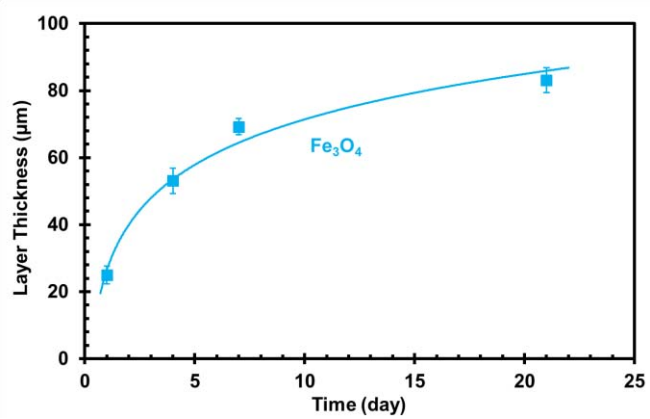

Figure 9. The thickness of Fe_3O_4 layer with time in the experiment without H_2S, T=120°C, initial pH=4.0.

The X65 steel specimen with preformed with Fe_3O_4 was exposed to a 0.1 bar H_2S under otherwise same conditions (Table 2) for another day. The EDS mapping results for the cross-sections are shown in Figure 10; all images are at the same magnification for ease of comparison. However, the data related to the experiment "with H_2S" were obtained using a different EDS detector than for the other two conditions and the display of the results can be more difficult to interpret. In the first row of Figure 10, the highest magnitude concentration of elements is indicated by white pixels and lowest magnitude by blue pixels; in the other two rows, the brightness intensity of the same-color pixels is related to the concentration. The level of color brightness can only be used in a qualitative way and can be compared from image to image. In terms of Fe_3O_4 layer thickness for the specimen with, without H_2S, and with preformed Fe_3O_4 layer, no significant difference can be found. However, the thickness of the outer iron

sulfide layer, represented by sulfur (S) content, greatly increased from less than 5 μm without the preformed Fe_3O_4 layer to 30 μm with the preformed Fe_3O_4 layer.

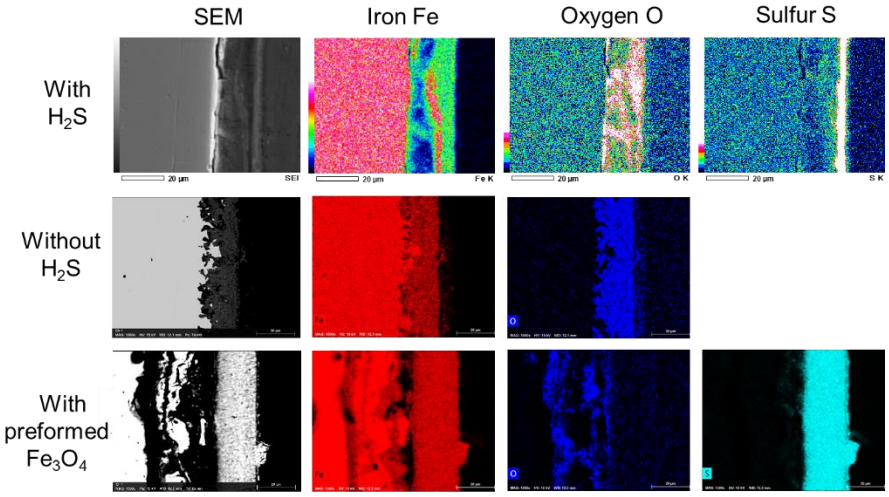

Figure 10. EDS mapping results for X65 specimen from the experiment without H_2S with, with 0.1 bar H_2S, and with preformed Fe_3O_4 layer, T=120°C, initial pH=4.0.

These experimental results infer that the formation rate of Fe_3O_4 is faster than that of iron sulfide at the tested temperatures. This explains why Fe_3O_4 is persistently detected while not being thermodynamically favored. In comparison, the presence of Fe_3O_4 was not reported at lower temperature in similar environments. A deeper look into the solubility limit of each corrosion product can help explain this behavior.

The solubility equilibria for Fe_3O_4 and mackinawite are given by Reactions (1) and (5) with the corresponding solubility limit expressions given by Equations (4) and (6). The effect of temperature on the solubility limit is shown in Figure 11. The solubility limit for Fe_3O_4 experiences a significant drop with the increase of temperature, while in comparison, for mackinawite, the decrease in solubility limit is only moderate.

$$Fe_3O_4 + 8H^+ \Leftrightarrow 2Fe^{3+} + Fe^{2+} + 4H_2O \quad (3)$$

$$K_{sp,Fe_3O_4} = e^{-\frac{\Delta G}{RT}} \quad (4)^{20}$$

$$FeS + H^+ \Leftrightarrow Fe^{2+} + HS^- \quad (5)$$

$$K_{sp,2} = 10^{\frac{2848779}{T_K} - 6.347 + \log(K_{a,1})} \quad (6)^{21}$$

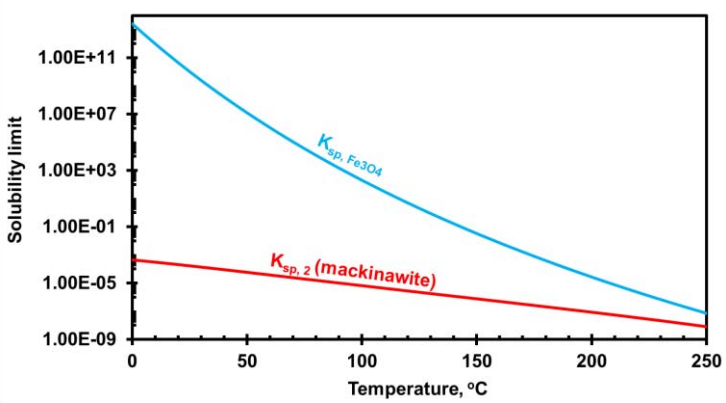

Figure 11. Solubility limit for Fe_3O_4 and mackinawite with the increase of temperature, pH=4.0, pH_2S=0.1 bar.

The level of saturation value governs the precipitation rate and consequently the layer formation/dissolution rate. The expressions for saturation value of Fe_3O_4 ($S_{Fe_3O_4}$) and mackinawite ($S_{mackinawite}$) are given in Equations (7) and (8). In this work, the ferric ion concentration [Fe^{3+}] was assumed to be 1.0×10^{-10} M, which means the calculated $S_{Fe_3O_4}$ may be underestimated compared to earlier similar studies[13].

$$S_{Fe_3O_4} = \frac{\frac{[Fe^{3+}]^2[Fe^{2+}]}{[H^+]^8}}{K_{sp,Fe_3O_4}} \tag{7}$$

$$S_{mackinawite} = \frac{\frac{[Fe^{2+}][HS^-]}{[H^+]}}{K_{sp,2}} \tag{8}$$

As soon as the steel specimen is inserted into an aqueous H_2S environment, iron starts to dissolve and release Fe^{2+}, resulting in an increase in pH (considering a closed system such as an autoclave). Figure 12 shows the changes in $S_{Fe_3O_4}$, bulk solution pH, and $S_{mackinawite}$ with an increase in [Fe^{2+}] from 0 to 10 ppm in a closed system. At 120°C with an initial pH 4.0, Fe_3O_4 is strongly supersaturated ($S_{Fe_3O_4}=10^6$) almost immediately after Fe^{2+} ions are generated in the solution. In contrast, $S_{mackinawite}$ requires at least 0.8 ppm of Fe^{2+} to reach a saturation of 1. Obviously, Fe_3O_4 is expected to precipitate faster and dominate the layer growth during the initial stage, because $S_{Fe_3O_4}$ is at least six orders of magnitude greater than $S_{mackinawite}$ and highly supersaturated. However, the solution pH will increase with time and this could change the ratio of saturation levels. Figure 12 also presents the saturation values at initial pH 5.0. However, the difference between initial $S_{Fe_3O_4}$ and $S_{mackinawite}$ is even higher at pH 5.0, so mildly acidic environments (pH 4 and pH 5) are not expected to largely affect the sequence and rate of layer growth at the tested temperature.

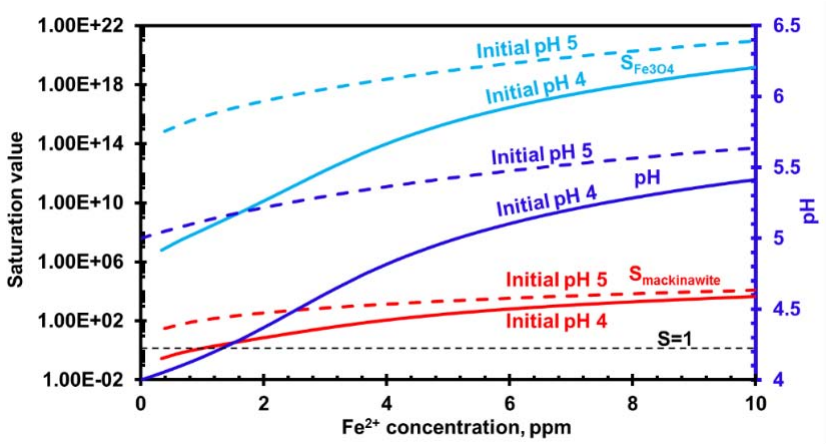

Figure 12. Saturation value for Fe_3O_4 and mackinawite at initial pH 4.0 and 5.0, $[Fe^{3+}]=1\times10^{-10}$ M, T=120°C, pH_2S=0.1 bar.

Figure 13 presents the trend of $S_{Fe_3O_4}$ and $S_{mackinawite}$ at 25°C and 120°C. It is important to notice that at 25°C and for very low ferrous ion concentrations, $S_{Fe_3O_4}$ is of the same magnitude as $S_{mackinawite}$. Considering that Fe_3O_4 is more soluble at lower temperatures (see Figure 11), this explains why Fe_3O_4 is not found at temperatures below 80°C while it forms very quickly and actually dominates during the initial stages of corrosion at temperatures above 80°C in an H_2S corrosion environment. Temperature is the key influential factor.

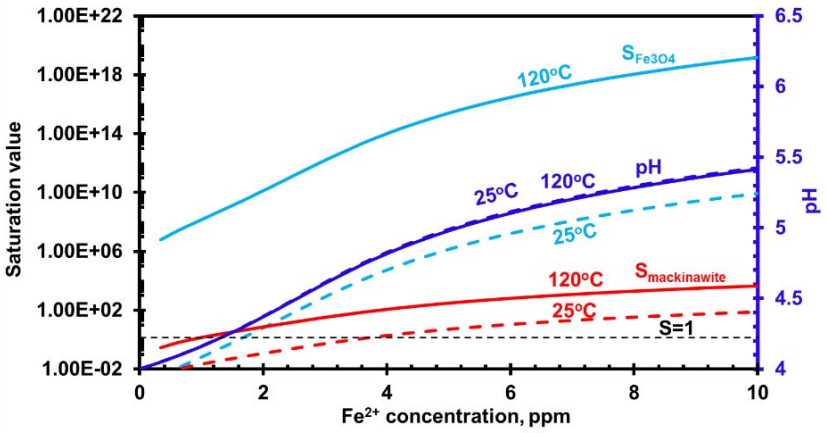

Figure 13. Saturation value for Fe_3O_4 and mackinawite at 25°C and 120°C, $[Fe^{3+}]=1\times10^{-10}$ M, pH_2S=0.1 bar, initial pH=4.0. (pH lines for 25°C and 120°C overlap in the graph)

In summary, due to a much higher saturation value, Fe_3O_4 is likely to form very quickly, faster than mackinawite, during the initial stages of corrosion at temperatures above 80°C in aqueous H_2S corrosion environments. It is hypothesized that Fe_3O_4 is responsible for the initial decrease in corrosion rate. A thin mackinawite layer is expected to immediately form as well when the steel is exposed to $[H_2S]_{aq}$.[12] Simultaneous growth of Fe_3O_4 and mackinawite is then expected to occur, but initially the kinetics for Fe_3O_4 precipitation dominates at high temperatures.

Iron Sulfide Formation Mechanism

After the initial stages of formation, the iron sulfide growth mechanism was investigated in Experimental Set #2 in order to test the 2nd hypothesis. The experimental design is shown in Figure 3. The Fe_3O_4

precipitation was performed on Ni specimens using Fe^{2+} ions generated by an independently corroding X65 steel specimens immersed in the same solution at 120°C, with an initial pH 4.0 and for 21 days. The Fe_3O_4 did indeed precipitate on the Ni surface, as identified by XRD in Figure 14. A precipitated Fe_3O_4 layer (~10 µm) can also be observed from the cross-section analysis in Figure 15 and is confirmed by the EDS mapping scan. This Ni specimen with the preformed Fe_3O_4 layer was then exposed for one day in a 0.1 bar H_2S environment under otherwise same conditions (120°C, initial pH 4.0) to verify the 2nd hypothesis.

After 1 day of exposure, the Ni specimen was retrieved and again characterized by XRD and SEM/EDS, as shown in Figure 14 and Figure 15. The Fe_3O_4 layer disappeared and was totally replaced by a mackinawite layer as confirmed by both XRD and EDS. The EDS mapping results show an iron sulfide layer on the Ni surface with no obvious oxygen (O) detected.

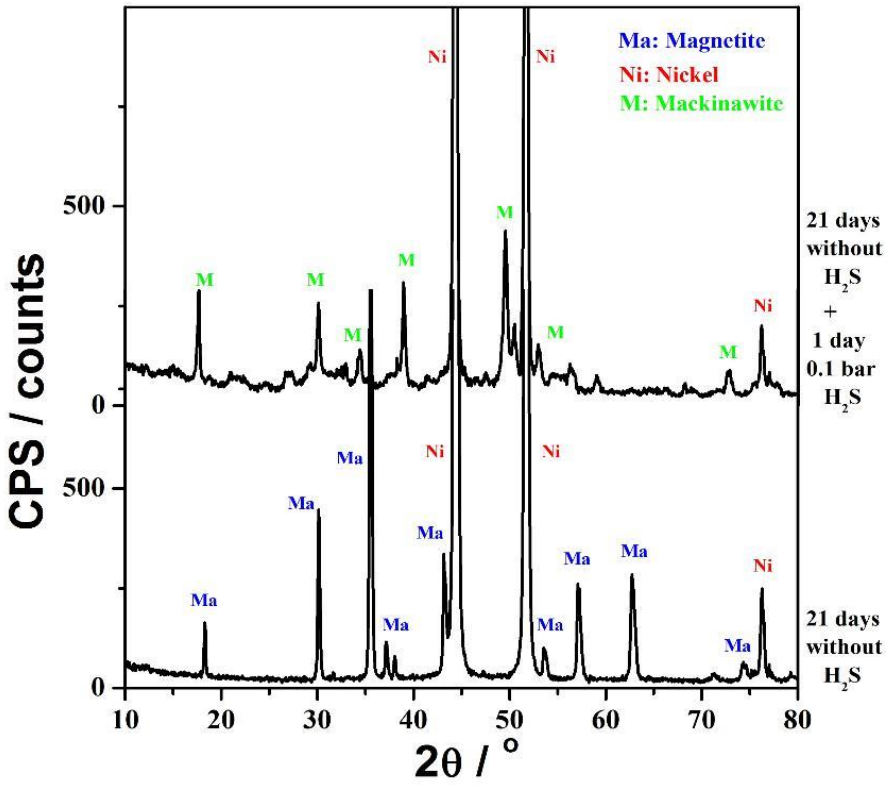

Figure 14. XRD patterns of preformed Fe_3O_4 layer on Ni specimen before and after H_2S was introduced, T=120°C, initial pH=4.0.

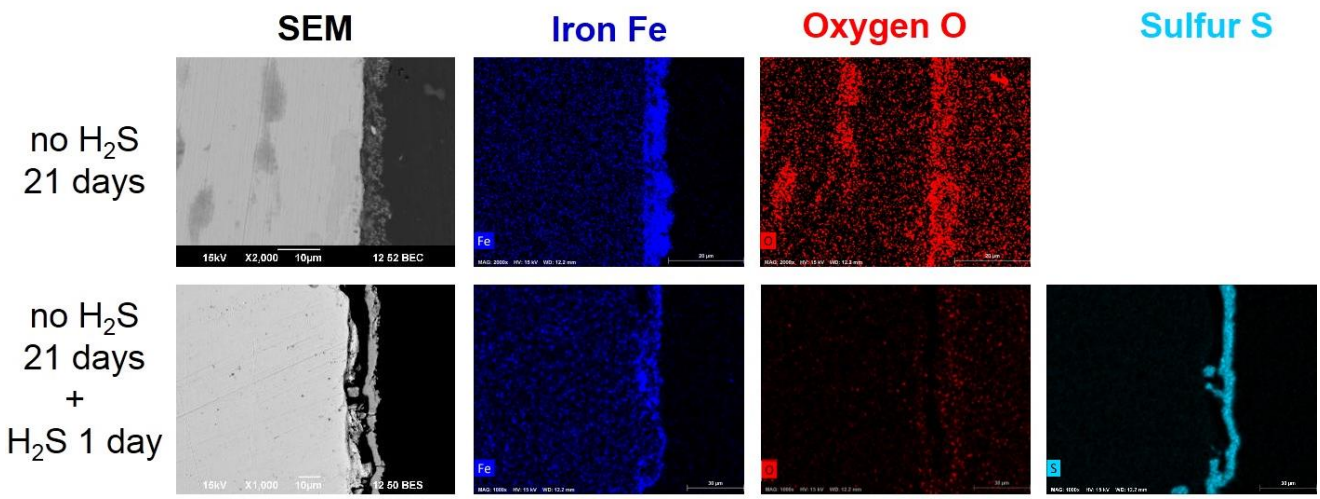

Figure 15. EDS mapping results for the cross section of preformed Fe_3O_4 layer on Ni specimen before and after H_2S was introduced, T=120°C, pH_2S=0.1 bar, initial pH=4.0.

The above results seem to validate 2nd hypothesis, stating that the FeS layer grows through Fe_3O_4 conversion. Without H_2S present, the Fe_3O_4 layer increased in thickness over time (Figure 9). With H_2S present, the Fe_3O_4 layer stabilized at a specific thickness while the iron sulfide layer increased in thickness with time due to the conversion reaction (Figure 1). Coincidentally, the FeS growth rate is similar to the rate of formation of the Fe_3O_4 layer observed in Figure 9. However, FeS precipitation via Reaction (5) cannot be entirely excluded since $S_{mackinawite}$ did exceed 1. However, previous results show that the Fe^{2+} concentration was around 3 ppm,[14] which gives a $S_{mackinawite}$ value around 10 (Figure 12). This value of saturation is not extremely high and would not constitute a high driving force to produce a significant amount of precipitated iron sulfide. A recent corrosion prediction model developed by Zheng, et al., [22] which includes iron sulfide precipitation, predicts the iron sulfide layer thickness to be below 14 µm after 7 days. Compared with the result in Figure 1, the thickness of iron sulfide was above 45 µm after 7 days. This further demonstrates that the main contribution to iron sulfide growth at higher temperatures was through the Fe_3O_4 conversion mechanism rather than the precipitation mechanism.

Descriptive Model for the Fe_3O_4/FeS Formation Mechanisms at High Temperature

Based on the experimental results, a descriptive model for Fe_3O_4 and FeS formation mechanisms at high temperature is presented in Table 3.

Table 3. Schematic diagrams for Fe_3O_4/FeS formation mechanisms at higher temperatures in a sour environment.

Step	Description	Schematic Diagram
(a)	X65 carbon steel is exposed to H_2S corrosion environment at high temperature. Fe starts to dissolve and releases Fe^{2+} ions in the solution.	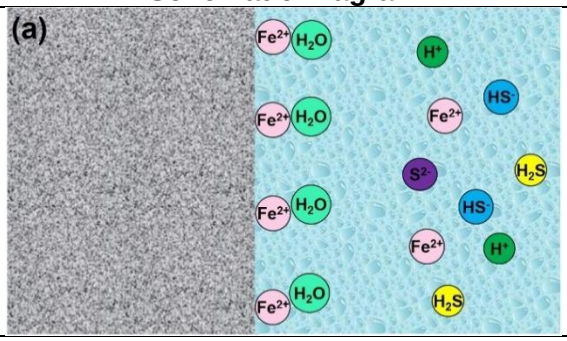
(b)	Fe^{2+} reacts with its surrounding H_2O molecules and Fe_3O_4 forms quickly via reaction (1). Fe_3O_4 layer is protective and the corrosion rate (i.e. the rate of Fe^{2+} ions release) decreases. Consequently, the formation rate of Fe_3O_4 also decreases which slows down the layer growth rate. Simultaneously, the aqueous H_2S reacts with the Fe_3O_4 layer, on the solution side, which transforms it to iron sulfide via Reaction (2) but initially at a much lower rate than Fe_3O_4 formation.	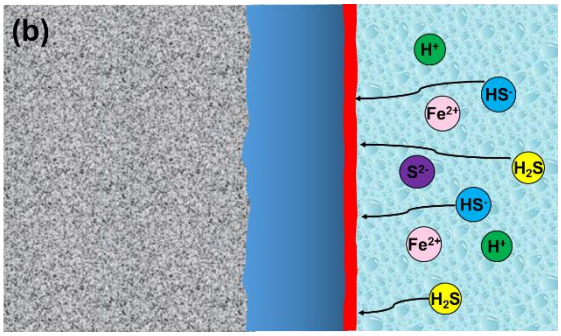
(c)	Iron sulfide formation through Fe_3O_4 conversion catches up as the formation of Fe_3O_4 slows down. Fe_3O_4 continuously forms at the metal surface and converts to iron sulfide at the Fe_3O_4/FeS interface; these two reactions occur at a similar rate which stabilizes the thickness of the Fe_3O_4 layer.	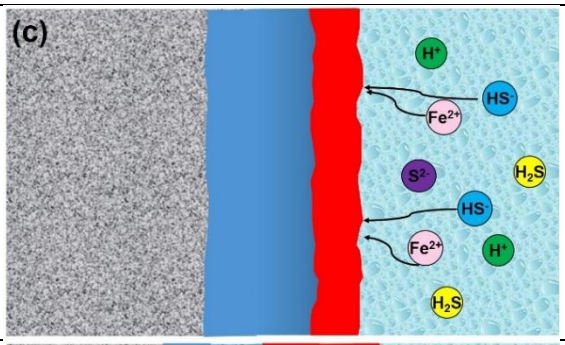
(d)	If the saturation value exceeds the solubility limit of iron sulfide, iron sulfide will precipitate at the FeS/solution interface and the FeS layer will grow even further.	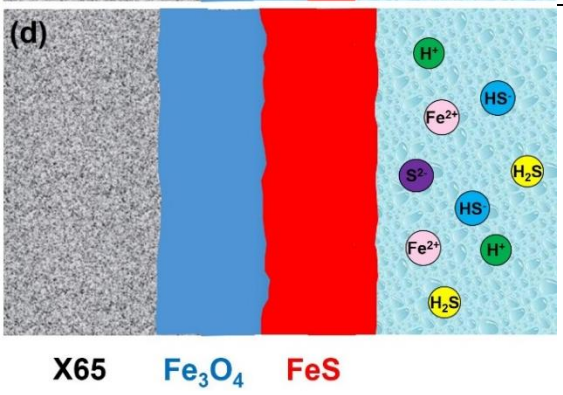

Other research studies[25-27] suggested alternative pathways for the layer growth mechanism, either stating that both Fe_3O_4 and FeS layers grow solely through precipitation (the present work suggests that precipitation is only a minor contributor) or postulating that the layer growth is linked to Fe solid state outward diffusion through the Fe_3O_4 lattice. However, the experimental results presented here do not seem to validate either of these mechanisms.

CONCLUSIONS

- Due to the faster kinetics at high temperature, a Fe_3O_4 layer is the dominant corrosion product forming at the steel surface in the initial stages of experiments where steel is exposed to an aqueous H_2S environment.
- Fe_3O_4 is responsible for the initial rapid decrease of the corrosion rate observed in sour environment at high temperature.
- Fe_3O_4 converts to mackinawite since it is thermodynamically less stable than iron sulfide. Fe_3O_4 experienced a simultaneous and continuous process of formation, at the steel/Fe_3O_4 interface, and transformation to FeS, at the Fe_3O_4/FeS interface.

ACKNOWLEDGEMENTS

The authors would like to express sincere appreciation to the following industrial sponsors for their financial support and direction: Anadarko, Baker Hughes, BP, Chevron, CNOOC, ConocoPhillips, DNV GL, ExxonMobil, M-I SWACO (Schlumberger), Multi-Chem (Halliburton), Occidental Oil Company, Petrobras, PTT, Saudi Aramco, Shell Global Solutions, SINOPEC (China Petroleum), TransCanada, TOTAL, and Wood Group Kenny.

REFERENCES

1. G. DeBruijin, “High-pressure, high-temperature technologies,” *Oilfield Review* 20, 3(2008): p. 46-60.
2. H.J. Chen, “High temperature corrosion inhibition performance of imidazoline and amide,” CORROSION/2010, paper no. 00035 (San Antonio, TX: NACE, 2010).
3. S.S. Prabha, “Corrosion problems in petroleum industry,” *European Chemical Bulletin* 3, 3 (2014): p. 300-307.
4. S. Gao, C. Dong, A. Fu, K. Xiao, X. Li, “Corrosion behavior of the expandable tubular in formation water,” *International Journal of Minerals, Metallurgy and Materials* 22, 2 (2015): p. 149-156.
5. S. Ramachandran, C. Menendez, V. Jovancicevic, J. Long, “Film persistency of new high temperature water-based batch corrosion inhibitors for oil and gas wells,” *Journal of Petroleum Exploration and Production Technology* 2, 3 (2012): p. 125-131.
6. J. Sun, C. Sun, X. Lin, X. Cheng, H. Liu, “Effect of chromium on corrosion behavior of P110 steels in CO_2-H_2S environment with high pressure and high temperature,” *Materials* 9, 3 (2016): p. 200.
7. B. Laurent, R. Harrington, B. Bennett, “Development of test methods and factors for evaluation of oilfield corrosion inhibitors at high temperature,” CORROSION/2017, paper no. 9780 (New Orleans, LA: NACE, 2017).
8. H. Mansoori, R. Mirzaee, F. Esmaeilzadeh, A. Vojood, A. Dowran, “Pitting corrosion failure analysis of a wet gas pipeline,” Engineering Failure Analysis 82, (2017): p. 16-25.
9. H. Ma, X. Cheng, G. Li, S. Chen, Z. Quan, S. Zhao, L. Niu, “The influence of hydrogen sulfide on corrosion of iron under different conditions,” *Corrosion Science* 42, 10 (2000): p. 1669-1683.
10. W. Sun, S. Nesic, S. Papavinasam, "Kinetics of iron sulfide and mixed iron sulfide/carbonate scale precipitation in CO_2/H_2S corrosion," CORROSION/2006*,* paper no. 06644 (San Diego, CA: NACE, 2006).
11. J. Tang, Y. Shao, J. Guo, T. Zhang, G. Meng, F. Wang, "The effect of H_2S concentration on the corrosion behavior of carbon steel at 90^{o}C." *Corrosion Science* 52, 6 (2010): p. 2050-2058.
12. Y. Zheng, B. Brown, S. Nesic, “Electrochemical study and modeling of H_2S corrosion of mild steel,” *Corrosion,* 70, 4 (2013): p. 351-365.
13. J. Ning, Y. Zheng, B. Brown, D. Young, and S. Nesic, “A thermodynamic model for the prediction of mild steel corrosion products in an aqueous hydrogen sulfide environment,” *Corrosion* 71, 8 (2015): p. 945-960.

14. S. Gao, P. Jin, B. Brown, D. Young, S. Nesic, M. Singer, “Corrosion behavior of mild steel in sour environments at elevated temperatures,” *Corrosion* 73, 8 (2017): p. 915-926.
15. S. Gao, P. Jin, B. Brown, D. Young, S. Nesic, M. Singer, “Effect of high temperature on the aqueous H_2S corrosion of mild steel,” *Corrosion* 73, 10 (2017): p. 1188-1191.
16. S. Gao, B. Brown, D. Young, M. Singer, “Formation of iron oxide and iron sulfide at high temperature and their effects on corrosion,” *Corrosion Science*, under review.
17. M. Liu, J. Wang, W. Ke, E. Han, “Corrosion Behavior of X52 Anti-H_2S Pipeline Steel Exposed to High H_2S Concentration Solutions at 90°C,” *Journal of Materials Science & Technology* 30, 5 (2014): p. 504-510.
18. R. Thodla, F. Gui, K. Evans, C. Joia, I. P. Baptista, “Corrosion fatigue performance of super 13 CR, duplex 2205 and 2507 for riser applications,” CORROSION/2010, paper no. 10312 (San Antonio, TX: NACE, 2010).
19. T. Tanupabrungsun, B. Brown, S. Nesic, “Effect of pH on CO_2 corrosion of mild steel at elevated temperatures,” CORROSION/2013, paper no. 2348 (Orlando, FL: NACE, 2013).
20. T. Tanupabrungsun, “Thermodynamics and kinetics of carbon dioxide corrosion of mild steel at elevated temperatures,” Ph.D thesis, Dept. of Chem. Eng., Ohio University, Athens, OH, 2013.
21. L.G. Benning, R.T. Wilkin, H.L. Barnes, “Reaction pathways in the Fe-S system below 100^{o}C,” *Chemical Geology* 167, 1 (2000): p. 25-51.
22. Y. Zheng, J. Ning, B. Brown, S. Neisc, “Advancement in predictive modeling of mild steel corrosion in CO_2- and H_2S-containing environments,” *Corrosion* 72, 5 (2016): p. 679-691.
23. E. Saaaoka, T. Ichio, S. Kasaoka, “High-Temperature H_2S Removal from Coal-Derived Gas by Iron Ore,” *Energy & Fuels* 6, 5 (1992): p. 603-608.
24. J. Ning, Y. Zheng, D. Young, B. Brown, S. Nesic, “Thermodynamic Study of Hydrogen Sulfide Corrosion of Mild Steel,” *Corrosion* 70, 4 (2014): p. 375-389.
25. T. A. Ramanarayanan, S. N. Smith, “Corrosion of iron in gaseous environments and in gas-saturated aqueous environments,” *Corrosion* 46, 1 (1990): p. 66-74.
26. P. Sarin, V. L. Snoeyink, D. A. Lytle, W. M. Kriven, “Iron corrosion scales: model for scale growth, iron release, and colored water formation,” *Journal of Environmental Engineering* 130, 4 (2004): p. 364-373.
27. T. Borch, A. K. Camper, J. A. Biederman, P. W. Butterfield, R. Gerlach, J. E. Amonette, “Evaluation of characterization techniques for iron pipe corrosion products and iron oxide thin films,” *Journal of Environmental Engineering* 134, 10 (2008): p. 835-344.